Geo-Mar Lett (2015) 35:161–174
DOI 10.1007/s00367-015-0398-2

ORIGINAL

Distinction and grain-size characteristics of intertidal heterolithic deposits in the middle Qiantang Estuary (East China Sea)

Daidu Fan · Shuai Shang · Guofu Cai · Junbiao Tu

Received: 17 October 2014 / Accepted: 15 January 2015 / Published online: 1 March 2015

Abstract The routine sampling procedure for grain-size analysis of intertidal heterolithic deposits runs a high risk of inadvertent mixing of two or more different sedimentation units, which would consequently complicate data interpretation. Traditionally, sedimentologists pay less attention to muddy layers due to a lack of internal structures, although the grain-size populations of such layers should encode more information on fine-mud flocculation processes than sandy layers. In this paper, individual muddy and sandy layers of nine short cores from the Da-Jian-Shan tidal flats of the middle Qiantang Estuary in the East China Sea, which experiences tidal bores, were sampled separately for grain-size analysis. A core taken at Huang-Jia-Yan from the lower estuary, not affected by tidal bores, served for comparison. A curve-fitting method was employed to decompose each grain-size distribution into two Gaussian populations. Cumulative plots indicate that intertidal sediments are mostly dispersed as intermittent and uniform suspension loads, traction loads being absent or very subordinate. This is conceivably linked to flows agitated by tidal bores, and to the highly dynamic nature of fine sand and coarse silt particles. Selective transport and deposition have produced three distinct sedimentation units, namely, tidal-bore deposits, tidal sandy deposits, and tidal muddy deposits. These can also be discriminated on bivariate plots of any two textural parameters. Shoreward attenuation of tidal flows is reflected in the gradual fining and thinning of sandy layers from lower-flat massive sands, through middle-flat hybrid deposits (alternations of massive sands and tidal rhythmites), to upper-flat tidal rhythmites. This gradient is also well represented in slightly decreasing (increasing) sorting and decreasing (increasing) proportions of the coarser (finer) hydraulic populations in the muddy layers. Although no corresponding trends are discernible in the hydraulic populations of the sandy layers, these can be distinguished on the basis of characteristic sedimentary structures. The floc limit and floc volume fraction, estimated from the modes and proportions of the finer hydraulic populations, are 8~10 μm (16 μm) and on average 41.73% (26.41%) for muddy (sandy) layers, respectively. The most plausible explanation is that the floc limit sensitively responds to subtle changes in the suspended sediment composition and the ambient hydraulic and hydrochemical settings. In comparison, the Huang-Jia-Yan core features blurred bedding and higher contents of fine mud and flocs, these being consistent with the weaker energy on the upper tidal flat of the lower estuary where neither tidal bores nor bigger waves occur.

D. Fan (✉) · S. Shang · G. Cai · J. Tu
State Key Laboratory of Marine Geology, Tongji University, Shanghai 200092, China
e-mail: ddfan@tongji.edu.cn

Introduction

Thin heterolithic bedding is characterized by regular alternations of sand and mud layers, or bioclastic and siliciclastic layers. This facies type is primarily abundant in tide-dominated environments, but is also found in lacustrine and fluvial environments (Reineck and Singh 1980; Flemming and Bartholomä 1995; Davis and Dalrymple 2012). Heterolithic beds form in response to alternations in the grain-size composition of supplied sediment and/or changes in current velocity. Consequently, their grain-size distributions (GSDs) are generally polymodal, embodying information on both provenance and hydraulic processes. In the case of intertidal flats, the source of the sediment is usually located in the adjacent main channel. GSDs of intertidal-flat deposits are therefore considered to be good encoders of hydraulic conditions (e.g., Fan et al. 2006, 2014; Chang et al. 2007; Law et al. 2013).

In tidal heterolithic deposits, distinct bedding planes separate individual sandy and muddy layers deposited during flood (ebb) and slack tides, respectively (Reineck and Singh 1980; Fan and Li

2002; Davis and Dalrymple 2012). To date, however, such layers have rarely been sampled separately for the purpose of grain-size analysis (e.g., Fan et al. 2012, 2014), although this is a prerequisite to examine texturally homogeneous units for genetically meaningful interpretations of grain-size data (e.g., Passega 1964; Hartmann and Flemming 2007). In practice, the routine procedure of subsampling thin sediment layers runs the high risk of inadvertently merging two or more laminae, especially in the case of mm-scale tidal rhythmites. Consequently, the resultant GSDs may display mixtures of two or more hydraulic populations in the form of bi- or multi-modal curves, thereby complicating their geological interpretation (e.g., Flemming 1988, 2007).

Mathematical modeling is a powerful tool to unravel different hydraulic component populations in a mixture (Weltje and Prins 2007; Weltje and Roberson 2012). Genetically meaningful partitioning of GSDs can be achieved by end-member modeling or curve-fitting procedures. Curve fitting is accomplished by comparing with specific mathematical curve functions, including Gaussian (Shih and Komar 1994), Weibull (Sun et al. 2002), and log-hyperbolic (Hartmann and Bowman 1993; Le Roux and Rojas 2007; Bartholdy et al. 2007). Weibull and log-hyperbolic distributions may fit some sediment distributions (e.g., coarse unimodal fluvial sediments) better than the Gaussian distribution (Kondolf and Adhikari 2000; Hajek et al. 2010). Other comparative studies did not find any particular advantage of the more complex distributions over simple normal distributions (Hill and McLaren 2001; Barusseau 2011). In practice, the Gaussian function is the most widely employed.

Flocs or aggregates contribute significantly to mass transportation and sedimentation on intertidal flats, as demonstrated by in situ measurements of suspended flocs, grain-size analysis of bed sediment, and numerical modeling (e.g., Chang et al. 2007; Chang and Flemming 2013; Hill et al. 2013; Law et al. 2013). The floc limit (i.e., diameter delimiting sortable silts from flocculated mud) and floc mass fraction (i.e., amount of material deposited as flocs) are two essential parameters for the identification of flocculated sediments (McCave et al. 1995; Curran et al. 2004; Milligan et al. 2007). Floc limits of 8~10 μm were initially identified by a marked deficiency of particles in this size interval (McCave et al. 1995; Chang et al. 2007), later expanded up to 22 μm by Molinaroli et al. (2009) who suggested that the floc limit was an inverse function of the clay/silt ratio and, hence, more variable than previously thought. Already Curran et al. (2004) had shown by inverse modeling that both the floc limits and mass fractions varied from tidal creeks to tidal flats in Willapa Bay, USA (cf. also Law et al. 2013). Indeed, flocculation is a complex sedimentary process with numerous controlling factors, including particle size and mineralogy, concentration of suspended sediment and organic matter, ambient turbulence, salinity and temperature (Kranck 1973; Shi 2010; Gao and Collins 2014).

In the present study, individual sandy and muddy layers of intertidal-flat deposits of the Qiantang Estuary of the East China Sea were sampled separately for laser-diffraction grain-size analysis. The Gaussian function was employed to decompose GSDs into two hydraulic component populations, and their respective modal size, sorting and proportion (fraction) were calculated. These data were integrated with information on bulk structural and textural compositions. Specific aims of this study were to (1) better understand hydraulic processes and products associated with semidiurnal tidal cycles on intertidal flats, (2) explore helpful methods to discriminate different tidal sedimentation units, and (3) provide a simple tool to estimate the floc limit and volume fraction of tidal-flat deposits.

Regional setting

With a total length of 600 km and a catchment area of 49,000 km^2, the Qiantang is the largest river in the Zhejiang Province of central eastern China. This river has mean annual water and sediment discharges of (respectively) 30×10^9 m^3 and 6.6×10^6 tons to Hangzhou Bay (Han et al. 2003; Fan et al. 2015). Due to the funnel shape of the bay, the mean tidal range increases strongly from <2 m at the mouth to ~5.5 m near Ganpu (Fig. 1; Fan et al. 2014, 2015). Upstream of Ganpu the tidal range decreases because of increasing friction by the shoaling and narrowing river channel. The tidal asymmetry of both current speed and phase duration increases sharply from Ganpu to Da-Que-Kou, where a large river-mouth bar forms a steep seaward-facing slope (Yu et al. 2012; Fan et al. 2014, 2015). As a result, the tidal front is intensely distorted to form a large breaking wave known as a tidal bore. During spring tides, tidal bores are usually initiated between Ganpu and Da-Jian-Shan (DJS in Fig. 1), grow toward a maximum between Da-Que-Kou and Yanguan, and then decay upstream until they finally disappear a short distance upstream of Wenyan. The landward limit of tidal penetration is at Lucibu (an artificial dam wall) approx. 280 km upstream of the bay mouth.

The Hangzhou Bay-Qiantang Estuary system can be subdivided into four reaches on the basis of sedimentary and geomorphic criteria (Fig. 1; Chen et al. 1990; Zhang and Li 1996; Fan et al. 2014). The upper estuary between Lucibu and Wenyan forms the tidally influenced, river-dominated reach, where the sediment along the thalweg is predominantly composed of gravely very coarse and coarse sand. The middle estuary between Wenyan and Ganpu is a mixed-energy reach characterized by tidal bores, featuring a highly sinuous, meandering channel with extensively developed mid-channel bars and intertidal flats, the thalweg sediment mostly consisting of fine sand and coarse silt. The lower estuary between Ganpu and Jinshan, coincident with the inner part of Hangzhou Bay, is the river-influenced tide-dominated reach

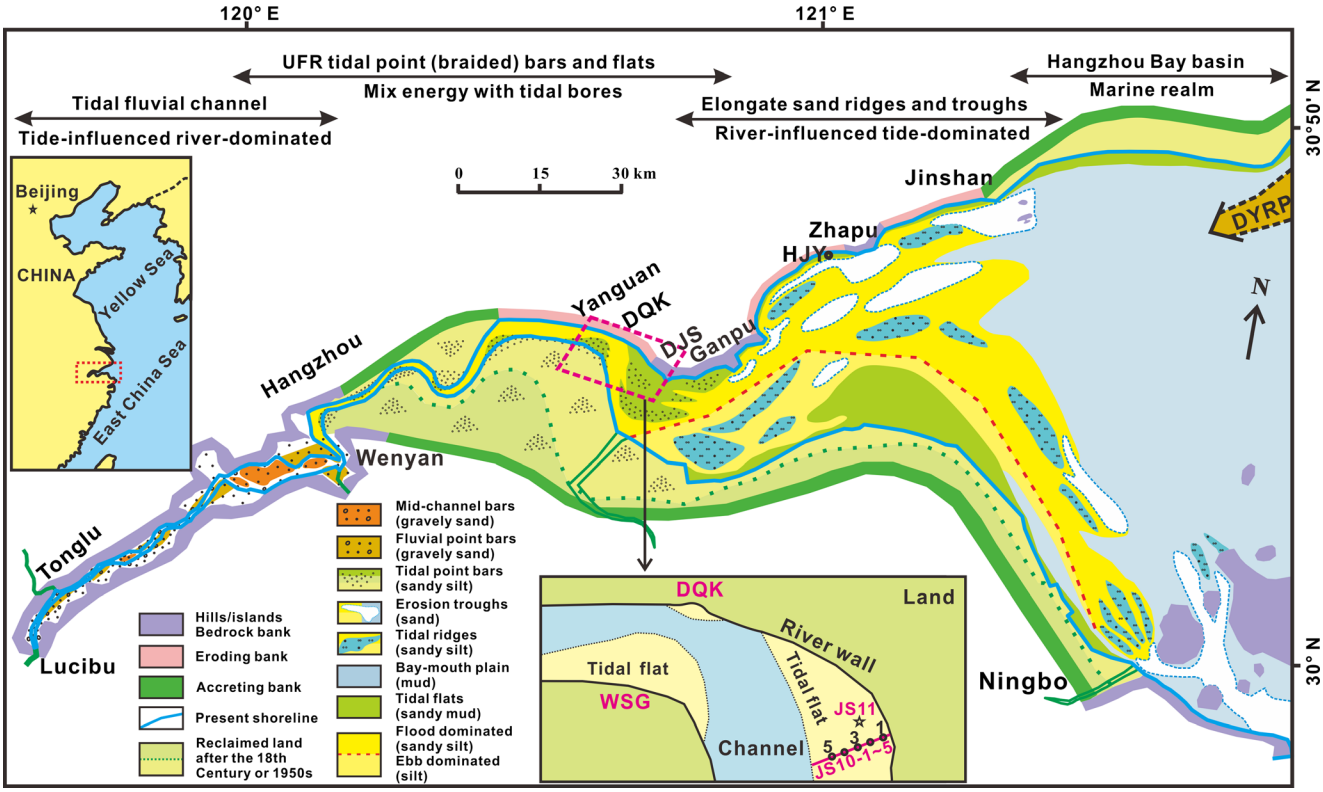

Fig. 1 Map showing the sedimentary facies distribution and coring locations in the Hangzhou Bay / Qiantang Estuary system. The tripartite subdivision includes (1) the upper, tide-influenced river-dominated reach, with coarse thalweg channel deposits, well-developed fluvial point bars, and mid-channel bars; (2) the tidal bore-affected middle reach comprising fine-grained sediments and featuring highly sinuous channels with tidal point bars; (3) the tide-dominated river-influenced outer reach, characterized by well-developed linear sand ridges and troughs (after Fan et al. 2014)

characterized by extensive longitudinal erosional troughs separated by accretionary ridges (Fig. 1). The outer part of Hangzhou Bay is formed by a relatively smooth muddy plain, the source of the mud being the Yangtze (Changjiang) River plume. As a consequence, it is considered part of the Yangtze subaqueous delta (Chen et al. 1990; Zhang and Li 1996; Han et al. 2003; Fan et al. 2012, 2014, 2015).

Materials and methods

In the middle Qiantang Estuary, five short cores (50~60 cm long) were collected on the accretionary tidal flats of DJS in 2010, numbered consecutively from JS10-1 on the upper tidal flat to JS10-5 on the lower tidal flat (Figs. 1, 2d; note: in Fan et al. (2012, 2014), the corresponding code is JS1 to JS5). Another four short cores (JS11-1 to -4, each ~100 cm long) were retrieved along an eroding cliff of the DJS marshland in 2011, numbered consecutively from JS11-1 at the cliff top to JS11-4 at the cliff toe (Figs. 2d, 3d). The short core HJY (~70 cm long) was collected in 2010 from the upper tidal flat of Huang-Jia-Yan in the lower Qiantang Estuary (Fig. 1), and served as a comparative example of intertidal areas not affected by tidal bores.

In the laboratory, the sediment cores were split lengthwise into two halves, and the surfaces of the working core halves were carefully smoothened with stainless steel knives to reveal any sedimentary structures. Individual sandy and muddy layers were sampled separately for grain-size analysis based on 423 samples, 82 from muddy and 341 from sandy layers. The samples were pretreated by adding 30% hydrogen peroxide and 10% diluted hydrochloric acid to remove organic matter and carbonate, respectively, followed by repeated washing with de-ionized water and then dispersal for a few minutes in an ultrasonic vibrator. Grain-size analyses were carried out by means of a laser-diffraction Beckman Coulter LS230, with a detection range of 0.375–2,000 μm.

Textural parameters were calculated using the moment method of Friedman and Johnson (1982). Grain-size data of cores JS10-1 to -5 and cores JS11-1 to -4 have served to discriminate tidal-bore deposits from regular tidal deposition in Fan et al. (2012, 2014, 2015). In this study, those data were recalculated to examine fine-scale variations in hydraulic processes and fine-grained mud flocculation processes on lower to upper intertidal flats.

The Gaussian function was employed to decompose each GSD into hydraulic component populations using the curve-fitting tool of the Matlab program. Size-frequency curves are

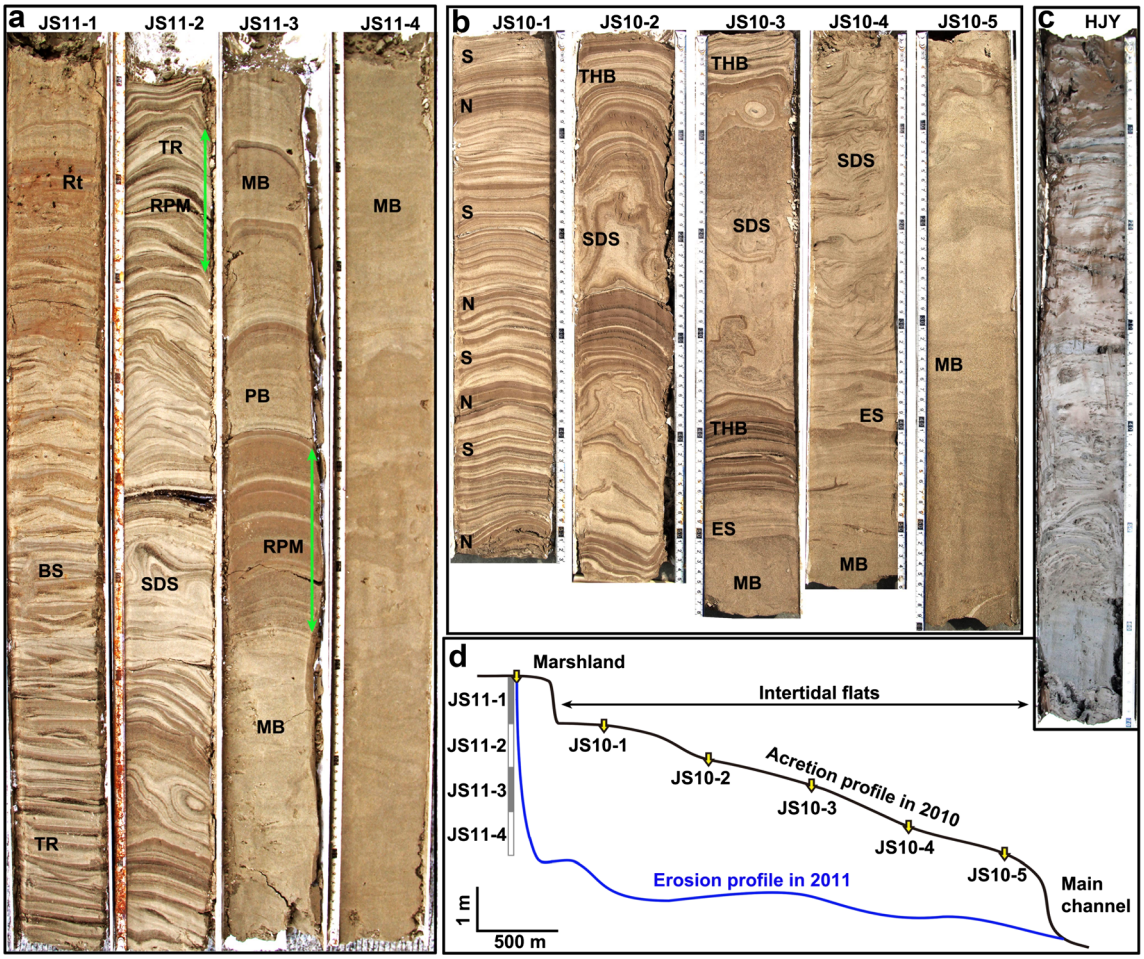

Fig. 2 Photographs of ten short cores retrieved from the DJS and HJY tidal flats. **a** Cores JS11-1 to -4 exhibit vertical stacked tidal-flat facies sequences along a roughly 4-m-high eroding cliff; **b** cores JS10-1 to -5 display lateral variations of tidal-flat facies along a central transect of the DJS tidal flats; **c** core HJY represents the lower estuarine environment characterized by higher water and mud contents with faint bedding surfaces; **d** sketch showing the coring locations on the DJS tidal flats. *Rt* Roots, *BS* burrow structures, *TR* tidal rhythmites, *RPM* rich in platy minerals, *SDS* soft-sediment deformation structures, *MB* massive bedding, *PB* parallel bedding, *THB* thin heterolithic beds, *ES* erosion structures, *S* spring tide, *N* neap tide

mostly quasi-unimodal distributions with significant fine-tail components. Coarse-tail components are usually negligible (<0.5%, i.e., five of 197 samples for cores JS10-1 to -5). Thus, the number of partitioning groups was set to two, and each GSD was decomposed into two component populations using the following equation:

$$f(x) = E\left[p_1 \frac{1}{\sigma_1\sqrt{2\pi}} \exp\left(-\frac{(x-m_1)^2}{2\sigma_1^2}\right) + p_2 \frac{1}{\sigma_2\sqrt{2\pi}} \exp\left(-\frac{(x-m_2)^2}{2\sigma_2^2}\right)\right]$$

where E is a constant representing the distribution density determined by the size class interval only, here 0. 135 φ for the laser-diffraction size analyzer; p_1 and p_2 are the percentages of the coarser and finer components based on their modal values, whereby $p_1 + p_2$ add up to 100%; m_1, m_2, and σ_1, σ_2 are the modal and sorting values of the two normally distributed component populations, respectively.

The output of component decomposition was examined by the Trust-Region algorithm in terms of the coefficient of determination (R^2) and the root-mean-square error (RMSE). R^2 was usually larger than 0.98. In contrast to coarser component populations having better sorting, finer component populations are poorly sorted, as would be expected for flocculated material. Therefore, floc limits and floc volume fractions were interpreted from the statistics of modal size and proportions of finer component populations of the analyzed GSDs.

Results

Structural characteristics

The five short cores JS10-1 to -5 recovered along the central transect of the DJS tidal flats show a gradual shoreward transition from massive sand to tidal rhythmites (Fig. 2b). Cores

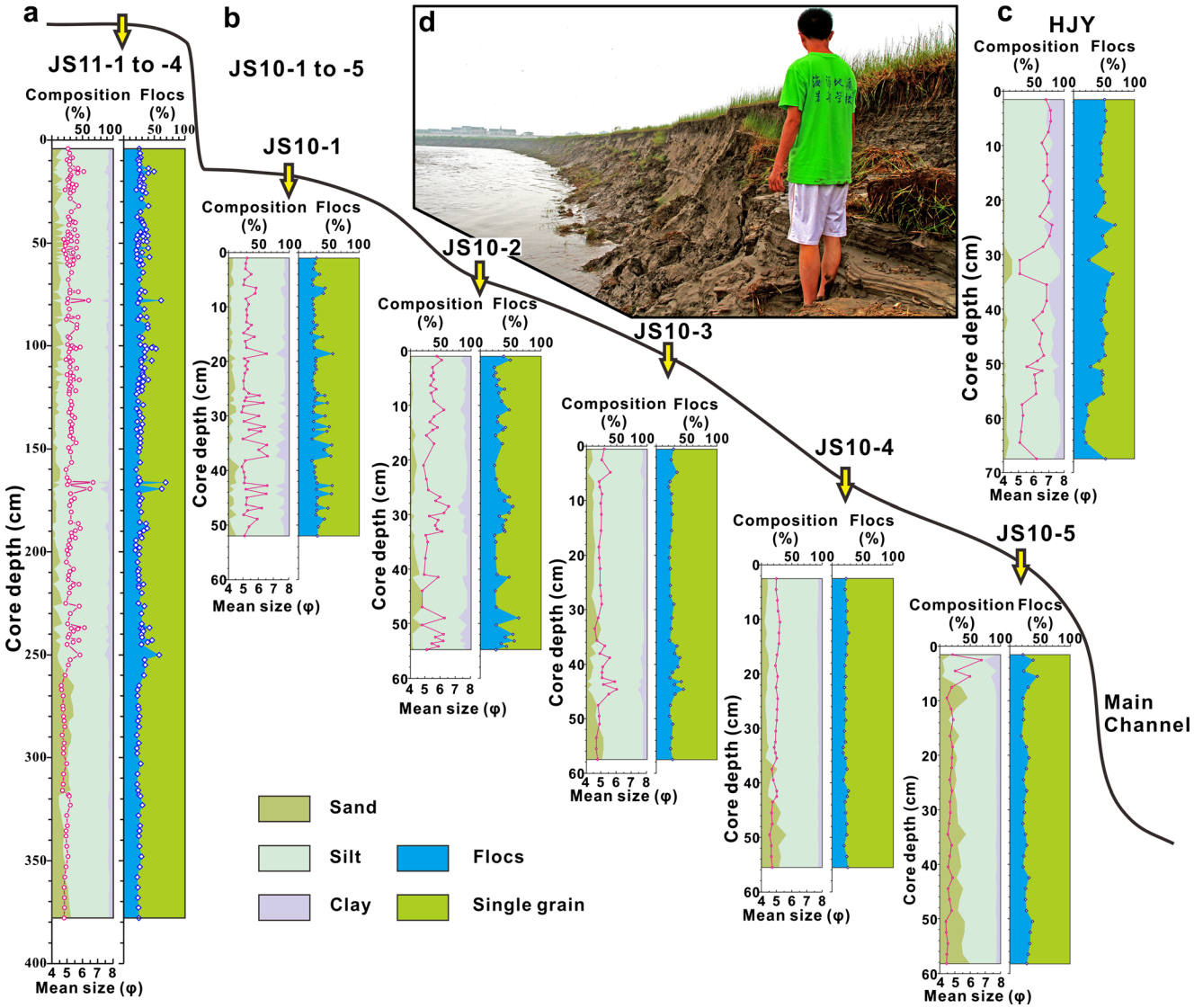

Fig.3 Grain-size compositions and estimated floc fractions along an intertidal transect; **a** cores JS11-1 to -4; **b** cores JS10-1 to -5; **c** core JHY; **d** photograph of the eroding cliff where cores JS11-1 to -4 were retrieved

JS10-4 and -5, located near the main channel, are mainly composed of massive sand with a few irregular deformation structures. Cores JS10-1 and -2 from the upper tidal flat feature alternations of sand-dominated and mud-dominated packages, the regular alternations of thickening and thinning sand-mud couplets in core JS10-1 being interpreted as representing spring-neap tidal cycles. Core JS10-3 displays a hybrid structural composition comprising thin heterolithic beds and thick sand beds composed of massive bedding units, parallel laminations and irregular deformation structures.

Sedimentary structures in cores JS11-1 to -4 from the eroding cliff show the same vertical sequence as observed along the transect in cores JS10-1 to -5, plus 30 cm of overlying marsh deposits. Some scattered burrows and plant roots occur in the upper tidal-flat and marsh deposits, respectively (Fig. 2a).

On the upper tidal flat of the lower estuary, core HJY shows completely different structures from those in the middle estuary (Fig. 2). In contrast to the clear lamination and bedding structures in the cores from the DJS tidal flats, core HJY is characterized by blurred bedding and a higher water content, with irregular sandy stringers and sand patches interspersed.

Textural characteristics

The DJS tidal-flat deposits are dominated by silt, which on average constitutes 78.51% (82.90%) of sandy (muddy) layers (Fig. 3). Mean sand and clay contents are 14.04% and 7.45% for sandy layers, and 3.12% and 13.98% for muddy layers, respectively. A maximum sand content of 49.52% was measured in a single “sandy” layer, and a minimum silt content of 68.34% in a single “muddy” layer. Therefore, the terms

"sandy" and "muddy" are here used in a loose sense to describe layers composed of two overlapping distributions, and distinguished by markedly different colors as well as structural and textural characteristics.

A general fining-upward trend is observed in all short cores, typically represented by an upward decrease in sand content (Fig. 3). The commonly observed shoreward-fining trend is particularly well recorded along the central transect of the DJS tidal flats, where cores JS10-5 to JS10-1 feature a gradual increase in both silt and clay contents of bulk sediments (Fig. 3b). A fining-upward trend is obvious in cores JS11-4 to JS11-1 (Fig. 3a), consistent with the attenuating tidal flow from the lower to upper tidal flats. In addition, core HJY has overall higher clay and lower sand contents than those of the DJS tidal flats (Fig. 3). This is plausibly linked with the lower-energy conditions reigning on the upper tidal flat of HJY in the inner part of the lower Qiantang Estuary, where neither tidal bores nor bigger waves occur.

Hydraulic component populations

All grain-size frequency curves are positively skewed (or fine skewed), deviating from a normal distribution with a tail of excess fine particles. Compared to muddy layers, sandy layers have a narrower and taller main population, as well as a smaller fine-tail component (Fig. 4).

Decomposing each sandy and muddy GSD into two normally distributed populations by means of the Gaussian curve-fitting function revealed that the two components of a given sandy or muddy layer have remarkably different modal and sorting values (Fig. 5, Table 1). The coarser-grained hydraulic populations (HPs) have a narrower sorting range (0.4–1.0 φ, with one exception at 1.29 φ) reflecting very well to well sorted sediments. The finer-grained HPs have a broader sorting range (approx. 1.6–2.5 φ) depicting poorly to very poorly sorted sediments. On the DJS tidal flats, sandy layers have slightly better sorted coarser-grained HPs and slightly less well sorted finer-grained HPs than muddy layers, the sandy and muddy layers being approximately separated along the B2 and B3 boundaries between the coarser and finer HPs in the sorting versus modal diameter scatter plot of Fig. 5. However, there is no clear demarcation between sandy and muddy layers in the corresponding data for core HJY. In this case, the distribution pattern resembles that of muddy layers on the DJS tidal flats (Fig. 5), being potentially linked with higher clay contents in both sandy and muddy layers of core HJY.

On the DJS tidal flats, the contribution of on average 73.59% of coarser HPs in sandy layers is roughly three times larger than that of finer HPs (26.41%). The corresponding values for muddy layers are 58.27% and 41.73%, respectively (Table 1). The difference in the proportion of coarser and finer HPs is minor in sandy layers of the HJY tidal flat, their relative contributions (55.42% vs. 44.58%) approximating that of muddy layers (52.27% vs. 47.73%).

In the bivariate plot of modal diameter versus proportion in Fig. 6, the coarser HPs of sandy layers on the DJS tidal flats form a tight group in accordance with their good sorting values. The coarser HPs of muddy layers scatter over a wide range, displaying a decreasing trend in their proportion as the sediment becomes finer (cf. increase in modal grain size expressed in phi units) shoreward from cores JS10-1 to JS10-5, or upcore from JS11-4 to JS11-1. The distributions of finer HPs in sandy and muddy layers crosswise mirror those of the coarser HPs, with a distinct boundary at a modal size of 6 φ (Fig. 6). Furthermore, trend variations are not clear for either coarser or finer HPs from sandy and muddy layers on the HJY tidal flat.

Discussion

Hydraulic interpretation

In the middle Qiantang Estuary, tidal-flat deposits are predominantly composed of fine sand and silt. These were inferred to

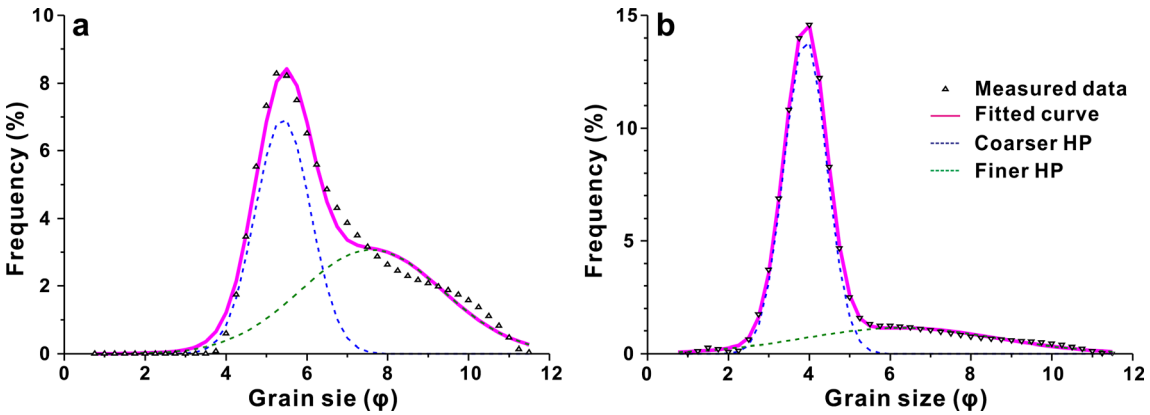

Fig. 4 Comparison between measured and simulated grain-size distributions of **a** representative muddy layers, and **b** representative sandy layers. *HP* Hydraulic population

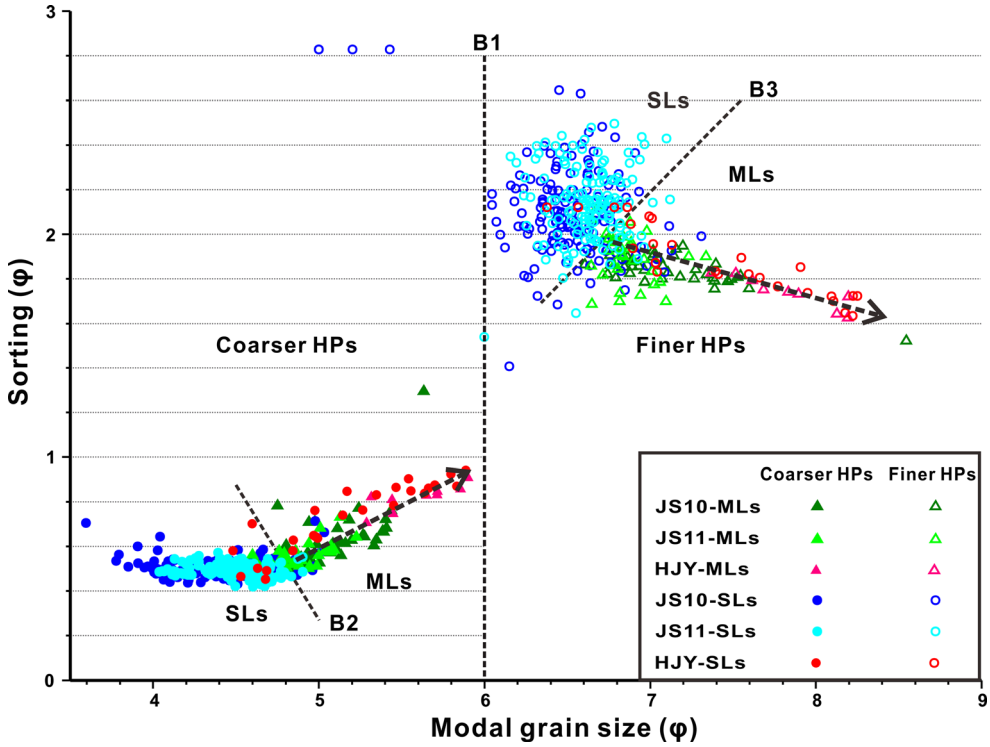

Fig. 5 Bivariate plots of modal grain size versus sorting of the coarser and finer hydraulic populations (HPs) in sandy and muddy layers (SLs vs. MLs). Arrows point toward the shore

be transported as suspension loads, with little traction loads being discernible in the cumulative plots (Fig. 7) as well as the C-M diagram of Fan et al. (2012). This is attributed, on the one hand, to the hydraulic nature of the sediments, in that fine sand and coarse silt are the most dynamic particle groups (Shields 1936), being transported as intermittent suspension loads whereas finer-grained mud is dispersed in uniform suspension. On the other hand, it is also attributed to the hydraulic processes active in the middle estuary, where intense turbulence and bottom shear stresses are produced by tidal bores and shooting flows during the flood tide. A sustained current speed of over 200 cm/s was recorded at the initial stage of tidal-bore arrival up to the beginning of the sharp velocity decrease in the late flood flow during a spring tide, this high-energy phase being accompanied by an abrupt increase in suspended sediment concentration (Fan et al. 2012, 2014, 2015). Sedimentation occurs during the subsequent stages when the flow decelerates as the rising tide inundates the middle and upper tidal flats. Consequently, a shoreward-fining sequence of intertidal facies is produced from thick massive sands on the lower flat, through hybrid deposits on the intermediate flat, to tidal rhythmites on the upper flat. This trend in structural and textural composition is evident not only along the central intertidal transect (cores JS10-5 to -1) but also in the vertically stacked profile of the DJS tidal flats (cores JS11-4 to -1; Figs. 2, 3).

The cumulative plots of the DJS tidal-flat deposits are essentially composed of two parts, a coarser-grained steep segment and a finer-grained gently sloping segment (A and B in Fig. 7). The transition between the two segments consists of a smooth curve, interpreted to result from a mixture of two overlapping normal populations (cf. Bein and Sass 1978; Viard and Breyer

Table 1 Statistical parameters of the coarser and finer hydraulic populations of sandy and muddy layers in Da-Jian-Shan and Huang-Jia-Yan (the latter within brackets) tidal-flat deposits

Layers	Range	Coarser hydraulic populations			Finer hydraulic populations		
		Mode (φ)	Sorting (φ)	Proportion (%)	Mode (φ)	Sorting (φ)	Proportion (%)
Sandy	Minimum	3.59 (4.48)	0.42 (0.45)	44.37 (31.68)	5.00 (6.38)	1.41 (1.63)	18.29 (17.57)
	Maximum	5.03 (5.89)	0.71 (0.94)	81.71 (82.43)	7.31(8.25)	2.83 (2.12)	55.63 (68.32)
	Average	4.45 (5.18)	0.50 (0.73)	73.59 (55.42)	6.56 (7.42)	2.12 (1.88)	26.41 (44.58)
Muddy	Minimum	4.60 (5.29)	0.50 (0.71)	31.56 (47.05)	6.61 (7.37)	1.52 (1.63)	24.62 (39.13)
	Maximum	5.63 (5.90)	1.29 (0.91)	75.38 (60.87)	8.55 (8.19)	2.13 (1.83)	68.44 (52.95)
	Average	4.99 (5.59)	0.60 (0.82)	58.27 (52.27)	7.01 (7.83)	1.86 (1.74)	41.73 (47.73)

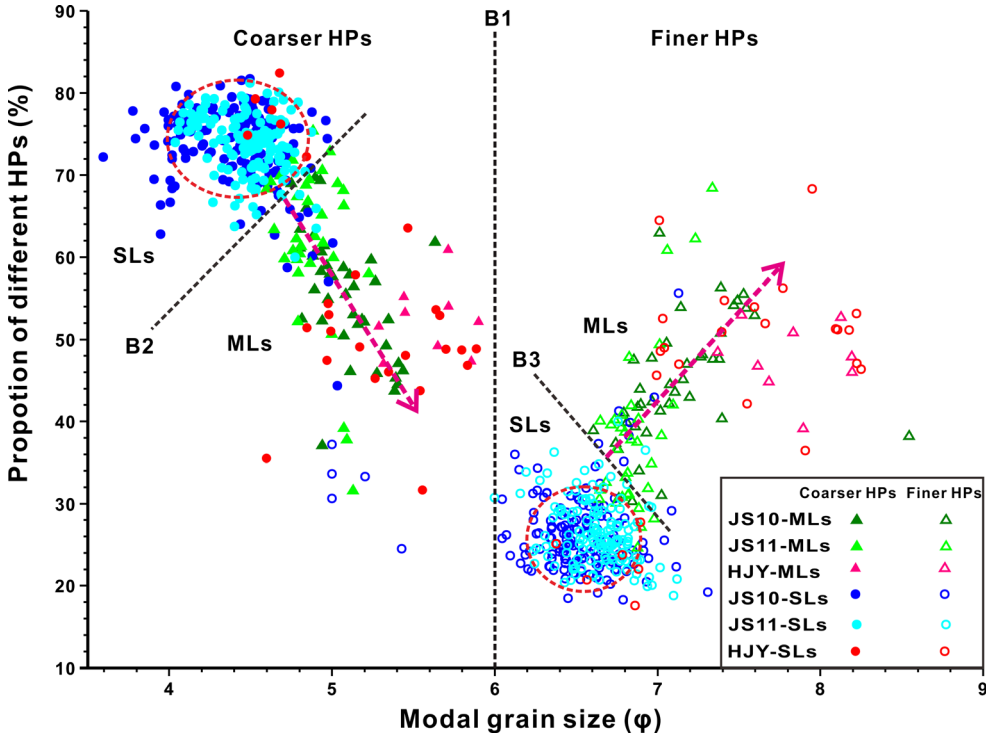

Fig. 6 Bivariate plots of modal grain size versus proportion of coarser and finer hydraulic populations (HPs) in sandy and muddy layers (SLs vs. MLs). Arrows point toward the shore

1979). This precisely corresponds to the decomposed hydraulic components (Fig. 4). The coarser-grained steep-segment component, associated with a narrow and steep normal population (coarser HP), represents an intermittent suspension load with particles having experienced selective transport before sedimentation, as indicated by their good sorting values (Fig. 5). By contrast, the finer-grained, gently sloping segment component, associated with a broader and flatter normal population (finer

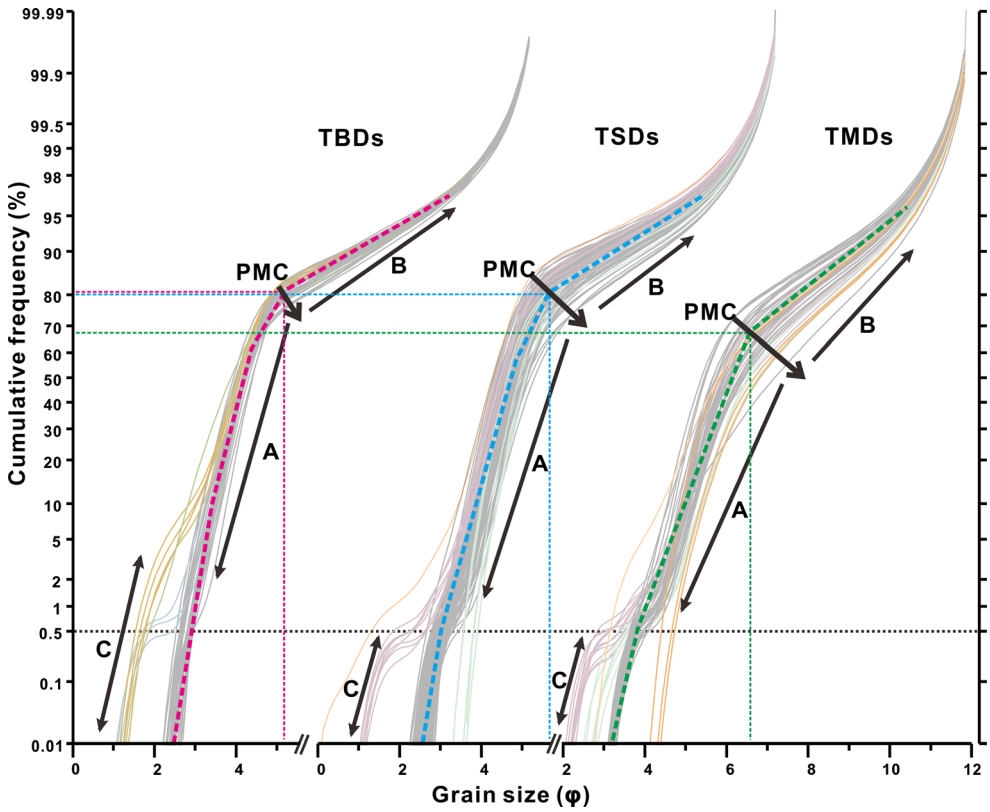

Fig. 7 Cumulative plots of sediment samples of tidal-bore deposits (TBDs), tidal sandy deposits (TSDs), and tidal muddy deposits (TMDs). Segments C, A and B represent different sediment transportation modes corresponding to traction, intermittent suspension and uniform suspension, respectively; *PMC* point of maximum curvature

HP), reflects uniform suspension transport with little sorting before sedimentation. In addition, there are some particles transported as traction load (C in Fig. 7), their contribution being usually less than 0.5%, with the exception of very few samples (five of 197) that reach 5~10%.

The point of maximum curvature (PMC) between the two segments of the cumulative plots potentially contains some hydraulic information on the two overlapping components (cf. Bein and Sass 1978). For example, the ordinate value of the PMCs is close to the percentage value contributed by the coarser-grained populations (Fig. 7, Table 1). Two kinds of sandy layers—tidal-bore deposits (TBDs) and tidal sand deposits (TSDs; cf. below)—have very similar ordinate values, these being much larger than those of the muddy layers. A shift toward finer grain sizes of the PMCs was observed in the shoreward direction for both sandy and muddy layers, reflecting the decreasing flow strength in that direction. All of the above findings attest to the usefulness of the method for obtaining hydraulic information, although the dissection of cumulative plots into straight-line segments for this purpose (Visher 1969; Viard and Breyer 1979) has remained controversial (Flemming 1988). In the present case, the data clearly support the procedure of Bein and Sass (1978) of subdividing such plots into smooth curve segments identifying two or more overlapping normal populations, instead of the truncated populations obtained in the procedure of Visher (1969).

It is generally accepted that sandy layers encode more hydraulic information than muddy layers because the latter are predominantly deposited as flocs during weak flow (e.g., Reineck and Singh 1980; Fan and Li 2002; Davis and Dalrymple 2012). Contrary to this understanding, bivariate plots of the component mode versus the proportion of sandy layers does not yield any more information, except for a clear demarcation from muddy layers (Fig. 6). However, the progressive shoreward fining of the modal sizes of coarser and finer HPs, accompanied by the increasing proportion of finer HPs in muddy layers, subtly reflect the shoreward attenuation of tidal flows across the intertidal flats. The same conclusion can be drawn from the scatter plot of the component sorting versus the modal diameter in Fig. 5. Thus, hydraulic component populations of muddy layers seem to be more sensitive in responding to subtle changes in tidal flows than those of sandy layers.

Discrimination of sedimentation units

Sandy layers on the DJS tidal flats appear to be deposited in two different ways. Thick sandy layers with an erosion base, and rich in massive bedding, graded bedding and/or soft-sediment deformation structures, are omnipresent on lower tidal flats directly impacted by tidal bores (Fig. 2). These have been ascribed to tidal-bore deposition, in that erosion surfaces and soft-sediment deformation of underlying strata are produced by the passage of tidal bores and shooting flood flows, after which rapid deposition occurs in the form of massive and graded bedding (Fan et al. 2012, 2014, 2015). By contrast, thin sandy layers are ubiquitous on the middle and upper tidal flats not directly influenced by tidal bores. Their thickness is generally less than 1 cm, besides being draped by thin muddy layers (Fig. 2). They are the product of regular tidal flows resulting in tidal sandy deposits (TSDs). Together with tidal muddy deposits (TMDs), three different sedimentary units have thus been identified on the DJS tidal flats.

The three units can also be distinguished by plotting any two textural parameters against each other. In the bivariate plot of sorting versus mean size in Fig. 8, the TSDs are located in the central lower part with intermediate mean sizes and the best sorting values. TBDs have coarser but less well sorted GSDs than TSDs because they are the product of rapid deposition from energetic tidal bores affecting the lower tidal flats, which contrasts with TSDs deposited from regular tidal flows over middle and upper tidal flats subject to selective transport before sedimentation (Fan et al. 2012, 2014). In comparison with TBDs and TSDs, TMDs feature the finest grain sizes and poorest sorting, having deposited from suspensions with a higher abundance of flocs produced during weak currents and slack tides. It is worth noting here that some sediment samples from the transitions between lower, middle and upper tidal flats deviate from the general discriminating patterns due to relative enrichment of platy minerals (RPM in Figs. 2, 8).

Bivariate plots of sorting versus skewness or kurtosis also demonstrate the different textural relationships of TBDs, TSDs and TMDs (Fig. 9). A negative linear relationship between these textural parameters was found in 197 samples from different sedimentation units in cores JS10-1 to -5 (Fan et al. 2012). This solid relationship was confirmed after adding 191 additional grain-size analyses from cores JS11-1 to -4, the resulting plots showing little change in both linear regression trends and correlation coefficients.

Bivariate plots of any two textural parameters are a potential tool for the discrimination of different sedimentation units in tide-dominated environments. This method has been widely and successfully employed to explore clues for depositional modes and sedimentary environments since the 1950s (e.g., Folk and Ward 1957; Friedman 1967), but it may fail in discriminating hydraulic conditions when grain-size distributions are multimodal. For example, Barusseau (2011) found no trend variations in the parametric relationships of beach sands among different morphodynamic zones along the northern coast of the Gulf of Lions. The successful discrimination achieved in the present study is therefore considered to be the result of strict adherence to the rule that sediment samples recovered for grain-size analysis should be retrieved from homogenous sedimentary units representing single or combined processes over defined periods of time (Passega 1964; Hartmann and Flemming 2007).

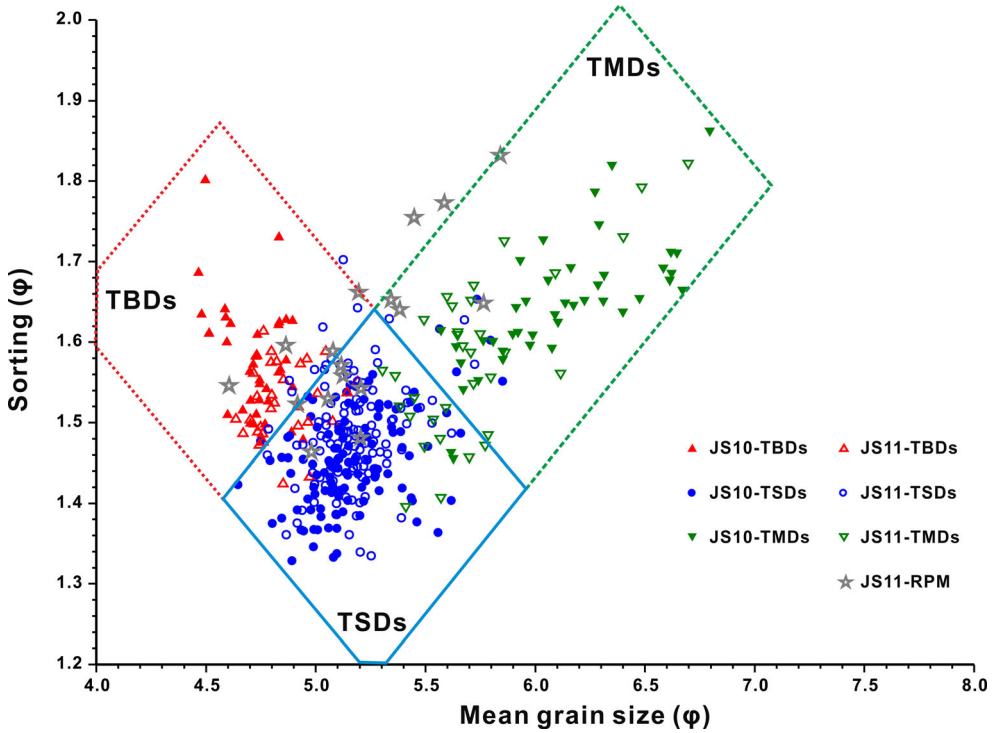

Fig. 8 Discrimination of the three different depositional units (*TBDs* tidal-bore deposits, *TSDs* tidal sandy deposits, *TMDs* tidal muddy deposits) identified in the study area on scatter plots of sorting versus mean grain size of the bulk sediment (modified from Fan et al. 2012, 2014)

Behavior and contribution of flocs

Flocculation has long been considered to govern the settling of fine-grained particles (e.g., Kranck 1973; McCave et al. 1995; Curran et al. 2004; Shi 2010; Chang and Flemming 2013; Gao and Collins 2014). Tidal-flat deposits in the Qiantang Estuary consist of large amounts of fine-grained muds (Fig. 3), and the distinction between sortable silts and flocs and/or aggregates is thus vital to the understanding of how heterolithic bedding is formed and accretion of tidal flats proceeds. Grain-size compositions of sedimentary units incorporate all particles, irrespective of whether they were deposited as single grains or flocs, and grain-size analysis is thus a powerful tool to obtain clues about floc limits and mass fractions. Floc limits can be diagnosed by a statistically significant deficiency of particles at the boundary separating two distinct mud populations when averaging frequency plots of all analyzed samples at discrete size intervals (McCave et al. 1995; Chang et al. 2007; Molinaroli et al. 2009). However, in the case presented here, this procedure failed because such a particle deficiency between the two component populations was not observed (Fig. 4). This is thought to be largely due

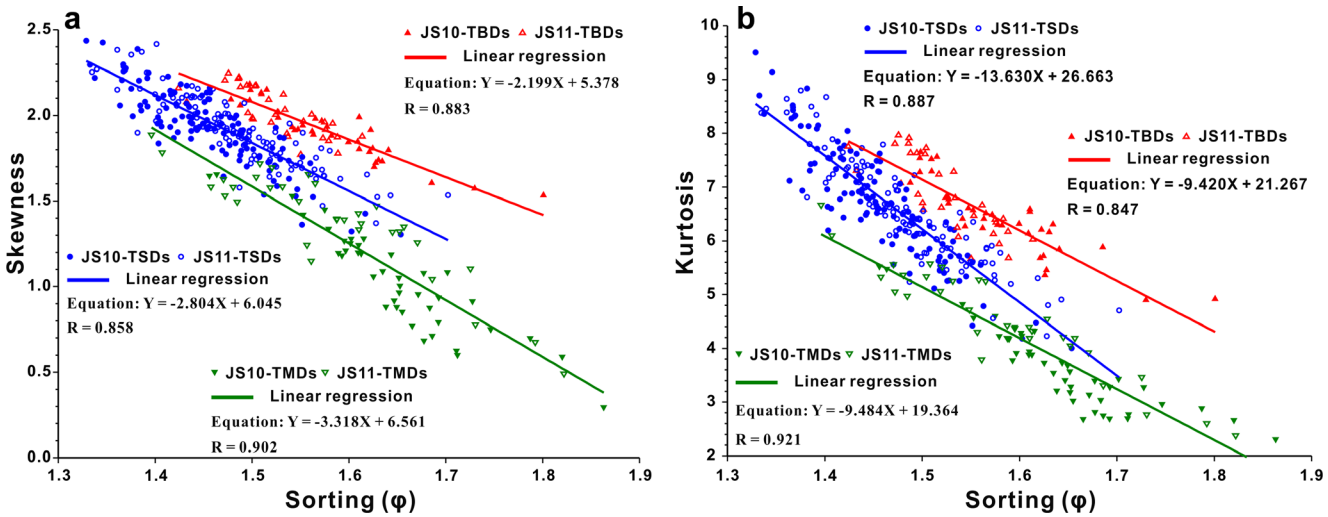

Fig. 9 Scatter plots of **a** skewness versus sorting and **b** kurtosis versus sorting, showing distinct grouping patterns of the three depositional units (*TBDs* tidal-bore deposits, *TSDs* tidal sandy deposits, *TMDs* tidal muddy deposits; adapted from Fan et al. 2012)

to the fact that the analyzed GSDs consist of two overlapping populations instead of truncated populations, which also accounts for the inflection shape of the cumulative plots (Fig. 7). Inverse models using a curve-fitting tool have been developed and employed to estimate floc limits and mass fractions. Thus, Curran et al. (2004) used a nonlinear least-squares fit to study flocculation in different environments (cf. also Milligan et al. 2007; Law et al. 2013). Because most of the GSDs in the present study consist of two normal populations, the Gaussian distribution fitting tool was employed to explore flocculation processes.

Numerical decomposition shows that the coarser and finer HPs differ remarkably in their modal diameter and sorting values (Table 1, Fig. 5). Coarser HPs are inferred to have been deposited as sortable silts based on their well sorted to very well sorted signatures, and grain-size modes in the medium–coarse silt range. In comparison, the finer HPs are primarily composed of fine–very fine silts deposited as flocs or aggreagates with poorly sorted to very poorly sorted values. However, the sorting interpretation based on grain-size measurements of fully dispersed sediment samples may conceal the fact that flocs and aggregates can be selectively transported and deposited as single (non-cohesive) particles, being hydraulically equivalent to syndepositional coarse silts and fine sands (cf. also Chang and Flemming 2013). Thus, the sorting value of finer HPs should reflect the genetic nature of flocs (i.e., the size range of particles being flocculated), rather than their transportation modes. In the above approach, floc fractions given by the proportion of finer HPs show distinct variations (Table 1, Fig. 3), on average contributing 41.73% to muddy layers and 26.41% to sandy layers. Each core was observed to display an upcore increase in the floc fraction, correspondingly seesawing over sandy and muddy layers. The remarkable shoreward increase in the floc fraction from the lower to upper tidal flats is evident both along the transect and the vertical profiles of cores JS10-5 to -1 and JS11-4 to -1 (Fig. 3). A similar phenomenon was reported from the intertidal sediments of Willapa Bay, USA (Law et al. 2013), where it was explained by the waning energy from lower to upper tidal flats, which is also reflected in the general fining trend of the sediment in the same direction. In addition, core HJY has much larger floc fractions than those of the DJS tidal flats, the former having a greater abundance of fine muds and weaker tidal flows typical of the lower Qiantang Estuary without tidal-bore action.

In the present study, the pronounced boundary between the coarser and finer HPs recorded at modal values around 6 φ (~16 μm; Figs. 5, 6) suggests that particles coarser or finer than 16 μm should be deposited as single grains or flocs, respectively, thereby defining an average floc limit. This floc limit is larger than the 8~10 μm suggested by McCave et al. (1995) and Chang et al. (2007), but still smaller than the maximum of 22 μm proposed by Molinaroli et al. (2009). Several factors may account for this discrepancy. For example, a laser particle sizer tends to overestimate the grain sizes of fine mud particles relative to those of other granulometric methods based on Stokes' sedimentation rate. Indeed, previous studies have shown that a laser-derived diameter of 16 μm might actually be equivalent to 10 μm when measured by a sedimentation method (Konert and Vandenberghe 1997; McCave et al. 2006). While this is a distinct possibility, it should also be taken into consideration that the assumption of a single discrete floc limit is questionable, given that flocculation/aggregation is a rather complex process influenced by numerous factors (Kranck 1973; Shi 2010; Gao and Collins 2014). In fact, muddy layers were found to have lower floc limits (8–10 μm; cf. boundary B3 in Figs. 5, 6) than sandy layers (16 μm). Law et al. (2013) also reported different floc limits from Willapa Bay, ranging from 9–10 μm on tidal flats to 16–18 μm in tidal creeks. Molinaroli et al. (2009) placed the floc limit in the Lagoon of Cabras at 8 μm, but at 22 μm in the Lagoon of Venice, the difference being attributed to the varying clay/silt ratios of roughly 1.0 in the low-energy Cabras as opposed to 0.3 in the higher-energy Venice lagoon. This suggests that the floc limit is a dynamic variable, which responds sensitively to subtle changes in suspended sediment compositions, as well as ambient hydraulic, hydrochemical and geomorphologic conditions.

Complex flocculation processes were further explored based on the relationship between the floc fraction and content of fine-grained mud (<16 μm). In Fig. 10 a clear boundary is observed at an abscissa value of 22%, which seperates the data points into two groups distinguished by different slopes of their respective linear regression curves. This division also roughly applies to the sandy and muddy layers of the DJS tidal-flat deposits in that only one of 73 muddy-layer samples—in striking contrast to 270 of 298 sandy-layer samples—has a fine-grained mud content below 22%. Core HJY has an elevated boundary value of 40% dividing sandy and muddy layers, consistent with the weaker energy conditions and greater abundance of fine-grained mud on that tidal flat. With the exception of six samples from the lower part of core HJY, which are similar to the sandy layers of the DJS tidal flats, the other samples scatter less regularly in the bivariate plot of Fig. 10. The latter were separately treated by linear regression analysis, together with the data from sandy and muddy layers of the DJS tidal-flat deposits. The high correlation coefficient and steep linear-regression slope for the sandy layers demonstrate that the fine-grained mud content is an essential factor controlling the floc fraction. Its impact decreases as fine-grained mud content increases above 22%, becoming negligible at values larger than 40–50%. This is considered to be associated with variations in turbulence and bottom shear stress during the deposition of different sedimentary units in various microenvironments. During formation of sandy layers, higher turbulence and bottom shear stress tend to

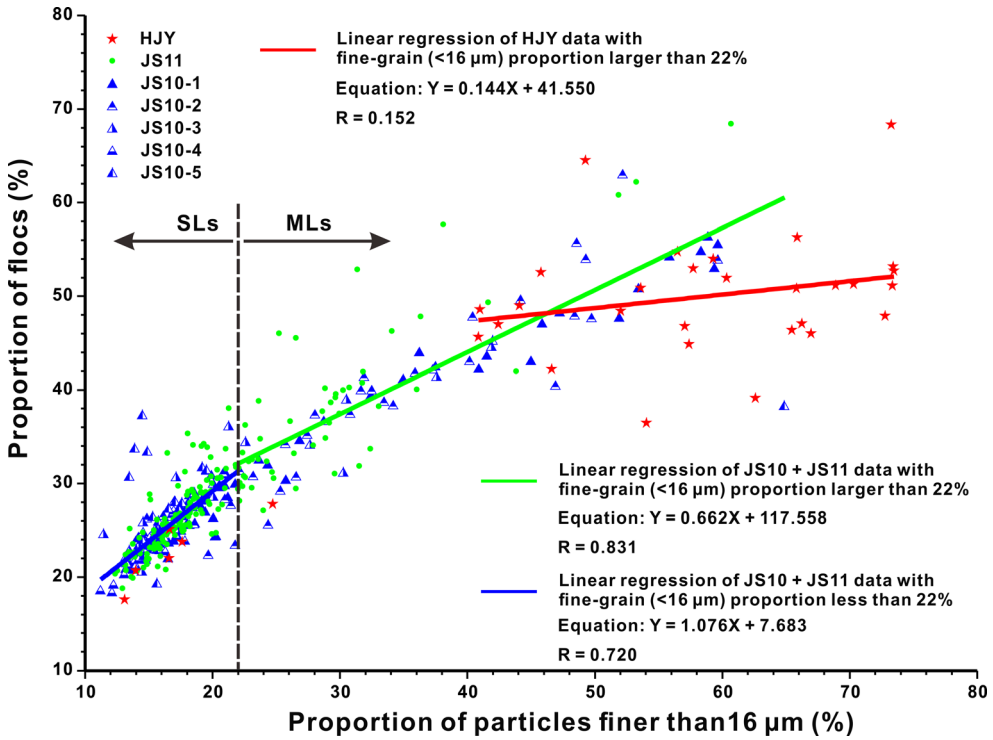

Fig. 10 Correlation between the floc fraction and the content of fine-grained (<16 μm) mud particles, showing different flocculation mechanisms during deposition of sandy and muddy layers, and also in different hydraulic conditions and sediment compositions

break up the aggregates of very fine-grained (<8 μm) mud particles, keeping these in suspension, whereas aggregates composed of fine silt particles (8–16 μm) survive and settle out together with fine sand and coarse silt particles, which results in an elevated floc limit of 16 μm (Figs. 5, 6). During the formation of muddy layers or, in more general terms, in less dynamic environments, the weak hydraulic conditions prevent size sorting of flocculated particles, which is further damped by massive flocculation. As a result, the flocculation process of very fine mud particles takes on a dominating role in controlling the settling of flocs, which becomes chaotic when the content exceeds 40–50% (Fig. 10). The above explanations await verification by additional field observations.

Conclusions

Sedimentary structures and grain-size distributions of individual layers of intertidal heterolithic deposits were examined in detail on material from ten short cores retrieved in the Qiantang Estuary. From the results, the following conclusions are drawn.

- Shoreward attenuation of tidal flow is associated with a gradual fining and thinning of sandy layers from massive sand on the lower tidal flats with tidal-bore influence, through alternations of massive sand and heterolithic rhythmites on the middle tidal flats, to regular tidal rhythmites on the upper tidal flats.
- Cumulative plots show that intertidal sediments are primarily transported as intermittent and uniform suspension loads, with little traction load, in response to flows agitated by tidal bores in the middle estuary.
- Differential transportation and deposition produce three distinct sedimentation units: tidal-bore deposits, tidal sandy deposits, and tidal muddy deposits, which can be discriminated in bivariate plots of any two textural parameters.
- Decomposition of grain-size distributions into a coarser and finer hydraulic population shows that the coarser populations of sandy layers are slightly better sorted than those of muddy layers, whereas the finer populations of sandy layers are slightly less well sorted than those of muddy layers. Notably, the sorting value of coarser populations reflects their transportation mode, whereas that of finer populations should represent the size range of flocculated/aggregated particles.
- The shoreward attenuation of tidal flows is also reflected by a slight decrease in sorting and progressively smaller proportions of coarser hydraulic populations in muddy layers, whereas the finer hydraulic population shows slightly better sorting and progressively increasing proportions.
- Floc limits and volume fractions, estimated from grain-size modes and proportions of the finer hydraulic population, were found to be 8–10 μm (16 μm) and on average

41.73% (26.41%) for muddy (sandy) layers, the difference in floc limit between sandy and muddy layers being attributable to different hydraulic conditions and fine-grained mud concentrations during deposition.

– Sandy layers provide vital clues about the dominant hydraulic processes active across intertidal flats, whereas muddy layers provide hints on subtle variations in both hydraulic and other ambient conditions—e.g., the ratio of sortable silt and flocculated mud. For the purpose of grain-size analysis, individual layers of heterolithic beds should therefore be sampled separately.

Acknowledgements This study was supported by the National Natural Science Foundation of China (NSFC) under grant numbers 41276045 and 41476031, the China Geological Survey (GZH201100203), and the Special Research Fund for the Doctor Program of Higher Education in China (20130072130003). We wish to thank Yijing Wu and Lingling Chen for their assistance in the field and with laboratory work. We also express our appreciation to two anonymous reviewers and the journal editors for their constructive suggestions on a previous version of the paper.

References

Bartholdy J, Christiansen C, Pedersen JBT (2007) Comparing spatial grain-size trends inferred from textural parameters using percentile statistical parameters and those based on the log-hyperbolic method. Sediment Geol 202:436–452

Barusseau JP (2011) Influence of mixtures of grain-size populations on the parametric and modal characteristics of coastal sands (Hérault, Mediterranean Sea, France). J Sediment Res 81:611–629

Bein A, Sass E (1978) Analysis of log-probability plots of recent Atlantic sediments and its analogy with simulated mixtures. Sedimentology 25:575–581

Chang TS, Flemming BW (2013) Ripples in intertidal mud—a conceptual explanation. Geo-Mar Lett 33:449–461. doi:10.1007/s00367-013-0339-x

Chang TS, Flemming BW, Bartholomä A (2007) Distinction between sortable silts and aggregated particles in muddy intertidal sediments of the East Frisian Wadden Sea, southern North Sea. Sediment Geol 202:453–463

Chen J, Liu C, Zhang C, Walker HJ (1990) Geomorphological development and sedimentation in Qiantang Estuary and Hangzhou Bay. J Coast Res 6:559–572

Curran KJ, Hill PS, Schell TM, Milligan TG, Piper DJW (2004) Inferring the mass fraction of floc-deposited mud: application to fine-grained turbidites. Sedimentology 51:927–944

Davis RA Jr, Dalrymple RW (eds) (2012) Principles of tidal sedimentology. Springer, Dordrecht

Fan D, Li C (2002) Rhythmic deposition on mudflats in the mesotidal Changjiang estuary, China. J Sediment Res 72:543–551

Fan D, Guo Y, Wang P, Shi JZ (2006) Cross-shore variations in morphodynamic processes of an open-coast mudflat in the Changjiang Delta, China: with an emphasis on storm impacts. Cont Shelf Res 26:517–538

Fan D, Cai G, Shang S, Wu Y, Zhang Y, Gao L (2012) Sedimentation processes and sedimentary characteristics of tidal bores along the north bank of the Qiantang Estuary. Chinese Sci Bull 57:1157–1167

Fan D, Tu J, Cai G, Shang S (2014) Characteristics of tidal-bore deposits and facies associations in the Qiantang Estuary, China. Mar Geol 348:1–14

Fan D, Tu J, Shang S, Chen L, Zhang Y (2015) Morphodynamics and sedimentary facies in a tidal-fluvial transition with tidal bores (the middle Qiantang Estuary, China). In: Tessier B (ed) IAS Spec Publ 48 (in press)

Flemming BW (1988) Process and pattern of sediment mixing in a microtidal coastal lagoon along the west coast of South Africa. In: de Boer PL, van Gelder A, Nio SD (eds) Tide-influenced sedimentary environments and facies. D Reidel, Dordrecht, pp 275–288

Flemming BW (2007) The influence of grain-size analysis methods and sediment mixing on curve shapes and textural parameters: implications for sediment trend analysis. Sediment Geol 202:425–435

Flemming BW, Bartholomä A (eds) (1995) Tidal signatures in modern and ancient sediments. IAS Spec Publ 24. Blackwell Science, Oxford

Folk RL, Ward WC (1957) Brazos River bar: a study in the significance of grain size parameters. J Sediment Petrol 27:3–26

Friedman GM (1967) Dynamic processes and statistical parameters compared for size frequency distributions of beach and river sands. J Sediment Petrol 37:327–354

Friedman GM, Johnson KG (1982) Exercises in sedimentology. Wiley, New York

Gao S, Collins MB (2014) Holocene sedimentary systems on continental shelves. Mar Geol 352:268–294

Hajek EA, Huzurbazar SV, Mohrig D, Lynds RM, Heller PL (2010) Statistical characterization of grain-size distributions in sandy fluvial systems. J Sediment Res 80:184–192

Han Z, Dai Z, Li G (2003) Regulation and exploitation of Qiantang River Estuary (in Chinese with English abstract). China Water Publication, Beijing

Hartmann D, Bowman D (1993) Efficiency of the log-hyperbolic distribution – a case study: pattern of sediment sorting in a small tidal-inlet – Het Zwin, The Netherlands. J Coast Res 9:1044–1053

Hartmann D, Flemming B (2007) From particle size to sediment dynamics: an introduction. Sediment Geol 202:333–336

Hill SH, McLaren P (2001) A comparison between log-hyperbolic and model-independent grain-size distribution in sediment trend analysis. J Coast Res 17:931–935

Hill PS, Newgard JP, Law BA, Milligan TG (2013) Flocculation on a muddy intertidal flat in Willapa Bay, Washington, Part II: observations of suspended particle size in a secondary channel and adjacent flat. Cont Shelf Res 60(supplement):S145–S156

Kondolf GM, Adhikari A (2000) Weibull vs. log-normal distributions for fluvial gravels. J Sediment Res 70:456–460

Konert M, Vandenberghe J (1997) Comparison of laser grain size analysis with pipette and sieve analysis: a solution for the underestimation of the clay fraction. Sedimentology 44:523–535

Kranck K (1973) Flocculation of suspended sediment in the sea. Nature 246:348–350

Law BA, Milligan TG, Hill PS, Newgard J, Wheatcroft RA, Wiberg PL (2013) Flocculation on a muddy intertidal flat in Willapa Bay, Washington, Part I: a regional survey of the grain size of surficial sediments. Cont Shelf Res 60(supplement):S136–S144

Le Roux JP, Rojas EM (2007) Sediment transport patterns determined from grain size parameters: overview and state of the art. Sediment Geol 202:473–488

McCave IN, Manighetti B, Robinson SG (1995) Sortable silt and fine sediment size/composition size slicing: parameters for palaeocurrent speed and palaeoceanography. Paleoceanography 10:593–610

McCave IN, Hall IR, Bianchi GG (2006) Laser vs. settling velocity differences in silt grain size measurements: estimation of palaeocurrent vigour. Sedimentology 53:919–928

Milligan TG, Hill PS, Law BA (2007) Flocculation and the loss of sediment from the Po River plume. Cont Shelf Res 27:309–321

Molinaroli E, Guerzoni S, De Falco G, Sarretta A, Cucco A, Como S, Simeone S, Perilli A, Magni P (2009) Relationships between hydrodynamic parameters and grain size in two contrasting transitional environments: the Lagoons of Venice and Cabras, Italy. Sediment Geol 219:196–207

Passega R (1964) Grain size representation by CM patterns as a geological tool. J Sediment Petrol 3:830–847

Reineck HE, Singh IB (1980) Depositional sedimentary environments, 2nd edn. Springer, New York

Shi JZ (2010) Tidal resuspension and transport processes of fine sediment within the river plume in the partially-mixed Changjiang River estuary, China: a personal perspective. Geomorphology 121:133–151

Shields A (1936) Application of similarity principles and turbulence research to bed-load movements (in German). Mitteilungen der Preussischen Versuchsanstalt für Wasserbau und Schiffbau, Berlin, Heft 26:3–26

Shih SM, Komar PD (1994) Sediments, beach morphology and sea cliff erosion within an Oregon coast littoral cell. J Coast Res 10:144–157

Sun D, Bloemendal J, Rea DK, Vandenberghe J, Jiang F, An Z, Su R (2002) Grain-size distribution function of polymodal sediments in hydraulic and aeolian environments, and numerical partitioning of the sedimentary components. Sedimentology 152:263–277

Viard JP, Breyer JA (1979) Description and hydraulic interpretation of grain size cumulative curves from the Platte River system. Sedimentology 26:427–439

Visher GS (1969) Grain size distribution and depositional processes. J Sediment Petrol 39:1074–1106

Weltje GJ, Prins MA (2007) Genetically meaningful decomposition of grain-size distributions. Sediment Geol 202:409–424

Weltje GJ, Roberson S (2012) Numerical methods of integrating particle-size frequency distributions. Comput Geosci 44:156–167

Yu Q, Wang Y, Gao S, Flemming B (2012) Modeling the formation of a sand bar within a large funnel-shaped, tide-dominated estuary: Qiantangjiang Estuary, China. Mar Geol 299:63–76

Zhang G, Li C (1996) The fills and stratigraphic sequences in the Qiantangjiang incised paleovalley, China. J Sediment Res 66:406–414